Korean J. Chem. Eng., 33(11), 3085-3101 (2016)
DOI: 10.1007/s11814-016-0198-z

pISSN: 0256-1115
eISSN: 1975-7220

Gas permeation and separation in asymmetric hollow fiber membrane permeators: Mathematical modeling, sensitivity analysis and optimization

Seyed Saeid Hosseini*,†, Javad Aminian Dehkordi*, and Prodip Kumar Kundu**

*Department of Chemical Engineering, Tarbiat Modares University, Tehran 14115-114, Iran
**OLI Systems, Inc, 240 Cedar Knolls Road, Suite 301 Cedar Knolls, NJ 07927-1621, U.S.A.
(*Received 21 April 2016 • accepted 2 July 2016*)

Abstract−Mathematical modeling is useful for analysis of process design and performance and is widely used for membrane separation and other important technologies in the energy sector. This study presents the results of our investigations on the mathematical modeling and optimization of hollow fiber membrane permeators specifically used for air separation as well as natural gas purification. The governing equations and mathematical models are developed based on the consideration of ideal and non-ideal conditions often involved in the separation of gas mixtures using membrane permeators. The influence and consequences of adoption of two distinct numerical methods for solving governing equations are investigated in details. The results obtained by using the models as well as the effect of numerical method type are examined and compared to the experimental data. The findings highlight the important role of the solution method on the validity and accuracy of the models. Moreover, the effect of variations in the operating conditions and physical geometries of the membrane are investigated through comprehensive sensitivity analysis. Accordingly, a set of optimal input parameters is determined using an appropriate statistical method. The findings provide useful information for the design and development of high performance membrane permeators and processes particularly in the case of binary gas mixtures for energy applications.

Keywords: Gas Separation, Hollow Fiber, Membrane Permeator, Mathematical Modeling, Sensitivity Analysis, Optimization, Numerical Method

INTRODUCTION

Polymeric membranes are known as an effective means for separation of various gas or liquid mixtures [1-4]. Low operation and energy costs, small footprint, reduced environmental side-effects and high reliability have turned membrane separation processes to a viable choice among the established rivals.

Many efforts have been made over the past years on design, fabrication, configuration, modeling, simulation and performance prediction and analysis in order to enable reliable membrane process developments [5-10]. Modeling of gas separation membranes was first reported by Weller and Steiner in 1950 [11]. Since then, numerous mathematical models have been introduced, especially for high flux asymmetric membranes with different flow configuration including co-current, counter-current and cross-current. Among the various membrane types and geometries, asymmetric hollow fiber membranes offer the advantages of high packing and area/volume density, reduced resistance to the transport of species as well as desirable mechanical strength and stability, particularly for gas separation applications [12]. In the prior studies, researchers considered pressure changes along the shell- and lumen-sides, real gas behavior and concentration polarization as influential parameters in order to develop more realistic mathematical models. Accordingly, a number of analytical and numerical techniques were examined to solve the derived formulae [13]. Despite the availability and widespread use of GEAR's method [14-16], Runge-Kutta [17-22] and orthogonal collocations [23-26], much attention has been paid to the use of finite difference methods for solving the equations. This may be attributed to the ease of formulation and simplicity, since depending on the prevailing conditions, other methods may offer either less accurate results with high computational time or limited stability and interval convergence [27-31]. Lim et al. [22] developed a model for analysis of pressure drop within the lumen-side of hollow fiber membranes based on continuity and momentum balance and used the Runge-Kutta method to solve the set of equations. In another study, Kaldis et al. [26] developed a modified model based on Pan's initial formulation [13] for prediction of membrane separation performance in asymmetric hollow fiber membrane modules and solved the final equations using orthogonal collocation. They took into account the temperature changes following the Arrhenius-type equation and employed Todus's method to calculate the variations of gas viscosity. However, the pressure changes in the shell- and lumen-sides as well as the resistance within the porous layer were neglected in their proposed model. It was determined that the model slightly overestimated the permeate concentration compared to the model proposed by Giglia et al. [17]. They also declared that orthogonal collocation offered more accurate solutions with less computational time [32].

Recently, authors developed mathematical models and investigated the effects of various parameters on the performance of asym-

†To whom correspondence should be addressed.
E-mail: saeid.hosseini@modares.ac.ir, seyedsaeidhosseini@gmail.com

metric hollow fiber membrane permeators for separation of binary gas mixtures [33,34]. Governing equations were developed and solved as a set of initial value problem equations using 4^{th}-order Runge-Kutta method. It was shown that the developed model based on non-ideal conditions offered better predictions about the module performance, and the deviation from ideality was considerably high. Despite the comprehensiveness of the developed models, one of the major shortcomings of employment of Runge-Kutta for solving the governing equations was the limited internal convergence especially in extending the model for analysis of the performance over a wide range of operating conditions.

Accordingly, the main objective of the present study was to employ the finite element method (FEM) for solving the governing equations to improve the accuracy and convergence and to overcome the limitations of the Runge-Kutta method. Based on a detailed literature review, and to the best of our knowledge, this is the first investigation that highlights the effect of adoption of numerical computation methods on mathematical modeling in the case hollow fiber membrane permeators for gas separation. In addition, the impacts of performing sensitivity analysis for identification of the pivotal parameters involved in the process design and performance were investigated in the case of O_2/N_2 and CO_2/CH_4 separation applications. The findings and proposed methodologies provide useful information about optimization of operating conditions and physical geometry parameters for design and development of high performance membrane permeators and processes.

THEORY AND MODEL DEVELOPMENT

To develop the mathematical formulae, a membrane module containing dead-end asymmetric hollow fiber membranes with determinate geometries was considered. It was assumed that streams flow in a counter-current mode and the permeate stream exits at the open-end of the hollow fibers. According to Fig. 1, feed stream enters at $z^*=0$ and the retentate exits at $z^*=1$.

The principal governing equations were derived considering both non-ideal and ideal conditions based on the following assumptions:

(1) Gas feed flows in the shell-side over the thin selective skin of the membranes.

(2) Resistance of the porous supporting layer against the flow is negligible.

(3) Diffusion along the pores is neglected due to the high permeation rate.

(4) No mixing of permeating species exists inside the porous supporting layer of the membranes.

(5) Deformation of the hollow fibers under pressure is negligible.

(6) The concentration of the permeate leaving the membrane skin surface (y′) is generally different from the bulk permeate stream outside the porous layer (y), except at the closed-end of the fiber where y′ and y are identical.

In terms of non-ideal conditions, real behavior of gas mixture in the shell- and lumen-sides was taken into account by engaging fugacity coefficients. Pressure changes at both shell- and lumen-sides were taken into account by employing appropriate equations. Pressure build-up at the lumen-side was calculated using the Hagen-Poiseuille equation, while that of shell-side was calculated using a differential equation derived from the mechanical energy balance [35]. The dependency of the membrane permeability to temperature was adjusted by using an Arrhenius-type relationship. Also, the dependency of gas viscosity to temperature, pressure and composition was taken into account by using the procedures described in the following sections.

Mass balance was applied for more and less permeable species in a binary gas mixture flowing over a differential element of hollow fiber membrane (dz) in a plug counter-current pattern. The equations were then combined and normalized followed by applying a local mass balance over the element to obtain a set of ordinary differential equations (ODE) representing the changes of molar flow rates of the retentate and permeate sides and the mole fraction of more permeable component at both sides of the membrane along the fiber. The resultant equations are as follows:

$$\frac{dU^*}{dz^*} = -K_1 P_F (Q_b/\delta)[\alpha(\phi_{11} x_s - \phi_{12}\gamma y') + \phi_{21}(1-x_s) - \phi_{22}\gamma(1-y')] \quad (1)$$

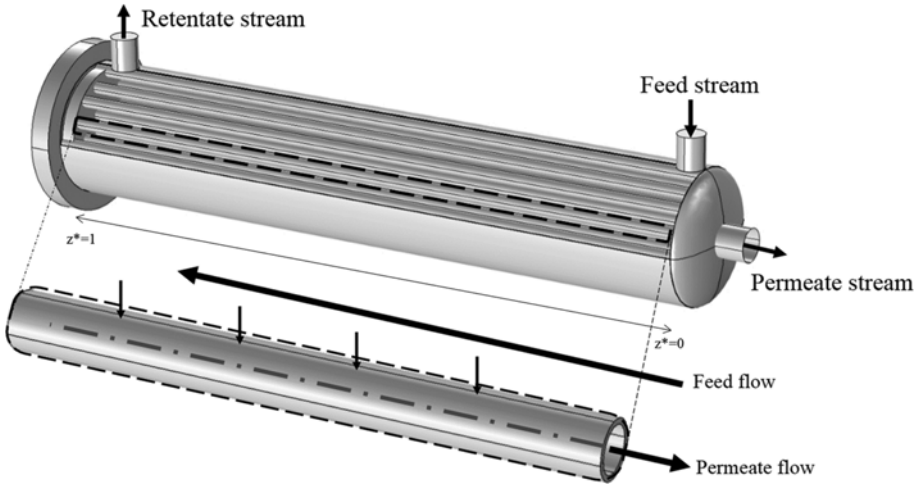

Fig. 1. Schematic representation of a hollow fiber membrane permeator module with counter-current flow configuration.

$$\frac{dV^*}{dz^*} = \frac{dU^*}{dz^*} \tag{2}$$

$$\frac{dx}{dz^*} = \frac{-K_1 P_F (Q_b/\delta)[\alpha(1-x)(\phi_{11}x_s - \phi_{12}\gamma y') - x(\phi_{21}(1-x_s) - \phi_{22}\gamma(1-y'))]}{U^*} \tag{3}$$

$$\frac{dy}{dz^*} = \frac{-K_1 P_F (Q_b/\delta)[\alpha(1-y)(\phi_{11}x_s - \phi_{12}\gamma y') - y(\phi_{21}(1-x_s) - \phi_{22}\gamma(1-y'))]}{V^*} \tag{4}$$

where U^*, V^* and z^* are dimensionless parameters defined as:

$$z^* = \frac{z}{L},\ U^* = \frac{U}{U_i},\ V^* = \frac{V}{U_i}$$

and K_1 is defined as:

$$K_1 = \frac{\pi d_o L N}{U_i}$$

In these equations, P_F, Q_b, δ, α, $\varnothing$, γ, d_o, L, N and U_i are feed pressure, permeability of less permeable component, effective skin thickness of membrane, membrane selectivity, fugacity coefficient, ratio of permeate-side pressure to feed-side pressure, fiber outer diameter, active fiber length, number of fibers in the module and feed flow rate, respectively.

The pressure changes along the fiber at feed and permeate sides were formulated as follows, respectively:

$$\frac{dP_F}{dz^*} = -\frac{2Z_F L R T_F f G^2}{P_F g_c R_h M w_m} \tag{5}$$

$$\frac{d\gamma}{dz^*} = \frac{K_2 \mu_P T_P V^*}{\gamma P_F^2} \tag{6}$$

where K_2 is defined as:

$$K_2 = -\frac{128 R L U_i}{\pi d_i^4 N}$$

and Z_F, R, T_F, G, Mw_m, μ_P and T_P are compressibility factor of gas mixture in the feed side, ideal gas constant, feed temperature, mass flux of feed side stream, molecular weight of gas mixture in the feed side, viscosity of gas mixture in the permeate side and permeate side temperature, respectively.

Also f, g_c and R_h are friction factor, Newton's law conversion factor and hydraulic diameter, respectively defined as:

$$f = 0.008(4R_h)^{-1/3} \text{ and } R_h = \frac{\pi(d_{s0}/2)^2 - N\pi(d_o/2)^2}{\pi d_{s0} + N\pi d_o}$$

where d_{s0} is the module shell diameter.

Applying a local mass balance equation together with mass balance equations for more and less permeable components after some simplifications yields Eq. (7):

$$y' = \frac{-\sqrt{[\varphi_{12} + \gamma(\alpha\varphi_{12} - \varphi_{22}) + x_s(\alpha\varphi_{11} - \varphi_{21})]^2 - 4\alpha\gamma\varphi_{11}(\alpha\varphi_{12} - \varphi_{22})x_s}}{2(\alpha\varphi_{12} - \varphi_{22})\gamma} \tag{7}$$

1. Model Development Based on Non-ideal Conditions

Many of the early conventional models for studying the properties and performance of asymmetric hollow fiber membranes generally ignored some or all of the non-ideal effects involved. This was either for the sake of simplification of the procedure and calculations or based on the assumptions prevailing in those specific cases [17,32,35-37]. Recent studies, however, have demonstrated that neglecting non-idealities in modeling can potentially cause serious errors in the evaluation or prediction of the process performance [15,38].

According to the experience gained in our research group on modeling of gas separation using hollow fiber membrane permeators [39,40], the major non-idealities and the procedure taken into considerations for model development are as follows:

(1) The SRK equation of state was used to calculate the fugacity coefficients to account for the real behavior of the gas mixtures [41].

(2) A surface mole fraction parameter was introduced for more permeable component using the equation proposed by Wang et al. [16] in order to consider the effect of accumulation of less permeable component adjacent to the membrane skin surface, which reduces the permeation driving force (also known as concentration polarization):

$$x_s = \frac{\alpha\varphi_{12}\gamma y'(1-x) - \varphi_{22}\gamma x(1-y') + x\left[\varphi_{21} + \dfrac{kT_0}{P_0 T_F\left(\dfrac{Q_b}{\delta}\right)}\right]}{\dfrac{kT_0}{P_0 T_F\left(\dfrac{Q_b}{\delta}\right)} + \alpha\varphi_{11}(1-x) + \varphi_{21}x} \tag{8}$$

where k, T_0 and P_0 are mass transfer coefficient in the feed side, standard temperature and standard pressure, respectively.

(3) Joule-Thomson equation was used to account for the effect of variation in the temperature of the components due to permeation. Also, the changes in the temperature of the feed stream along shell-side were calculated via the equation derived from the enthalpy balance and thermodynamic [42].

$$\mu_{JT,m} = \frac{\sum_{i=1}^{2} x_i C_{pi} \mu_{JTi}}{\sum_{i=1}^{2} x_i C_{pi}} \tag{9}$$

where C_p and μ_{JT} are the molar heat capacity at constant pressure for a pure component and Joule-Thomson coefficient, respectively.

(4) The dependency of permeation to temperature owing to the temperature changes at the feed side was considered by using an Arrhenius-type equation [38,40]:

$$Q = Q_{Ref} \exp\left[-\frac{E}{R}\left(\frac{1}{T_F} - \frac{1}{T_{Ref}}\right)\right] \tag{10}$$

(5) Temperature, pressure and concentration dependency of gas mixture viscosity were taken into account using the methods proposed by Chung et al., Jossi et al. and Wilke [43].

2. Model Development Based on Ideal Conditions

Model development was also carried out based on ideal conditions to enable having quick results without involving numerous non-ideal parameters and associated complexities. For this purpose, three more assumptions were taken into account for development of governing equations in addition to the former six assumptions considered for non-ideal conditions:

(1) Ideal behavior of gas mixtures ($\varphi=1$).

(2) The pressure changes on both sides of fiber are negligible (γ=constant and $\mu_{Feed}=\mu_{Permeate}$).

(3) The process is isothermal (α=constant).

By applying the above assumptions to Eqs. (1)-(4) and (7), the following equations were obtained for the ideal conditions. These equations represent the changes of molar flow rates of more permeable component in feed and permeate sides (Eqs. (11) and (12)), the changes in mole fraction of more permeable component in the feed and permeate sides (Eq. (13) and (14)) as well as local permeate side mole fraction of the more permeable component in the support layer (Eq. (15)), respectively as follows:

$$\frac{dU^*}{dz^*}=-\frac{\pi d_o LN(Q_b/\delta)P_F}{U_i}[\alpha(x-\gamma y')+(1-x)-y(1-y')] \tag{11}$$

$$\frac{dV^*}{dz^*}=\frac{dU^*}{dz^*} \tag{12}$$

$$\frac{dx}{dz^*}=-\frac{\pi d_o LN(Q_b/\delta)P_F}{U_i}\frac{[\alpha(1-x)(x_s-\gamma y')-x((1-x)-\gamma(1-y'))]}{U^*} \tag{13}$$

$$\frac{dy}{dz^*}=-\frac{\pi d_o LN(Q_b/\delta)P_F}{U_i}\frac{[\alpha(1-y)(x_s-\gamma y')-y((1-x)-\gamma(1-y'))]}{U^*} \tag{14}$$

$$y'=\frac{1+(\alpha-1)(\gamma+x)-\sqrt{[1+(\alpha-1)(\gamma+x)]^2-4\alpha\gamma(\alpha-1)x}}{2(\alpha-1)\gamma} \tag{15}$$

The overall and partial mass balances for the more permeable component are derived as follows, respectively:

$$U|_{z^*=0}=U|_{z^*=1}+V \tag{16}$$

$$x|_{z^*=0}U|_{z^*=0}=x|_{z^*=1}U|_{z^*=1}+yV \tag{17}$$

3. Numerical Solution by Finite Element Method

Finite element is a widespread and useful numerical method, especially for solving ordinary and partial differential equations. We adopted the Galerkin method to approximate the solution of ODEs with a piecewise linear function as a sum of basis functions [44]. By transforming a set of ODEs into a system of algebraic equations, the finite element method and a weak formulation of the approximation was used according to the prescribed procedure [45].

Considering a system of non-linear first order ODEs over interval (0 L), the following equation can be defined:

$$P'=f(P, z) \tag{18}$$

expanding an approximation solution using basis functions yields to P and P′ as follows:

$$P=\sum_{j=1}^{N}p_j\phi_j(z) \tag{19}$$

$$P'=\sum_{j=1}^{N}p_j\phi_j'(z) \tag{20}$$

where $\phi_j(z)$ is the hat function defined as:

$$\phi_j(z)=\begin{cases}0 & z\le z_{j-1}\\ \dfrac{z-z_{j-1}}{z_j-z_{j-1}} & z_{j-1}\le z\le z_j\\ \dfrac{z_{j+1}-z}{z_{j+1}-z_j} & z_j\le z\le z_{j+1}\\ 0 & z\ge z_{j+1}\end{cases}$$

Accordingly, the residual equation is:

$$R(z)=P'-f(P', z)=\sum_{j=1}^{N}p_j\phi_j'(z)-f(P, z) \tag{21}$$

It is desirable to minimize the residual equation, (i.e., R(z)=0). Thus, Eq. (21) is obtained by applying the weak Galerkin formulation of approximate solution as weight factors:

$$\int\phi_i(z)R(z)dz=0 \tag{22}$$

Finally, the Gauss quadrature formulae were used as the solution method. The boundary conditions rely on the flow pattern. The set of boundary conditions used in this study is provided in Table 1. In addition, Fig. 2 demonstrates the algorithms and calculation procedures followed for solution of models based on non-ideal and ideal conditions.

4. Sensitivity Analysis and Optimization

Sensitivity analysis provides useful information about the relationship between the involved variables. In addition, statistical methods reflect the interactions among the parameters and the role and contribution of each [46]. A conventional method of analyzing the sensitivity of a model is changing an independent variable while maintaining others unchanged. A strategic method for analyzing the relationships of the parameters in a process is to apply response surface methodology (RSM) [47]. We used central composite design (CCD) method to gain a response surface model and performed sensitivity analysis and optimization [48]. The statistical models were obtained using the Design-Expert 7.0 software. Input parameters were divided into two main categories. Feed

Table 1. The set of boundary conditions employed for solving ODEs

Model type	Position	Condition
The model based on non-ideal conditions	$z^*=0$	$U_i=1$
	$z^*=0$	$x=x_F$
	$z^*=0$	$y=y_0$
	$z^*=0$	$\gamma=\gamma_0$
	$z^*=0$	$P_F=P_{F0}$
	$z^*=1$	$V^*=0$
The model based on ideal conditions	$z^*=0$	$U_i=1$
	$z^*=0$	$x=x_F$
	$z^*=0$	$y=y_0$
	$z^*=1$	$V^*=0$

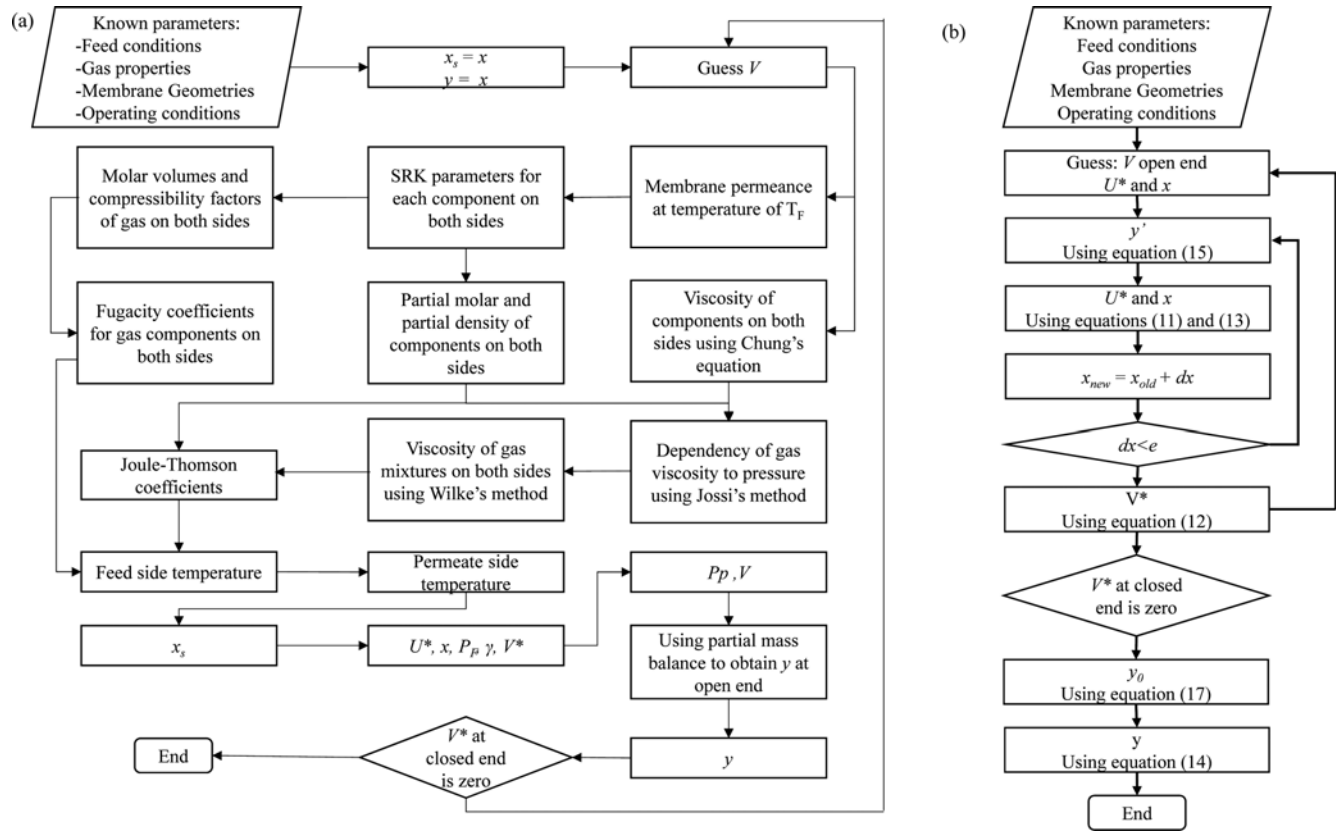

Fig. 2. The algorithms and calculation procedures used for solution of (a) the model developed based on non-ideal conditions (b) the model developed based on ideal conditions.

pressure, temperature and composition were classified as operating conditions, whereas fiber inner diameter, module diameter, number of fibers and active fiber length were classified as physical geometries of the membrane. Aiming for practical applications, the optimum operating conditions and physical geometries were evaluated and compared in the case of selected experimental data reported in literature [49].

RESULTS AND DISCUSSION

1. Grid Independency Check

A grid independency check was performed to ensure that numeri-

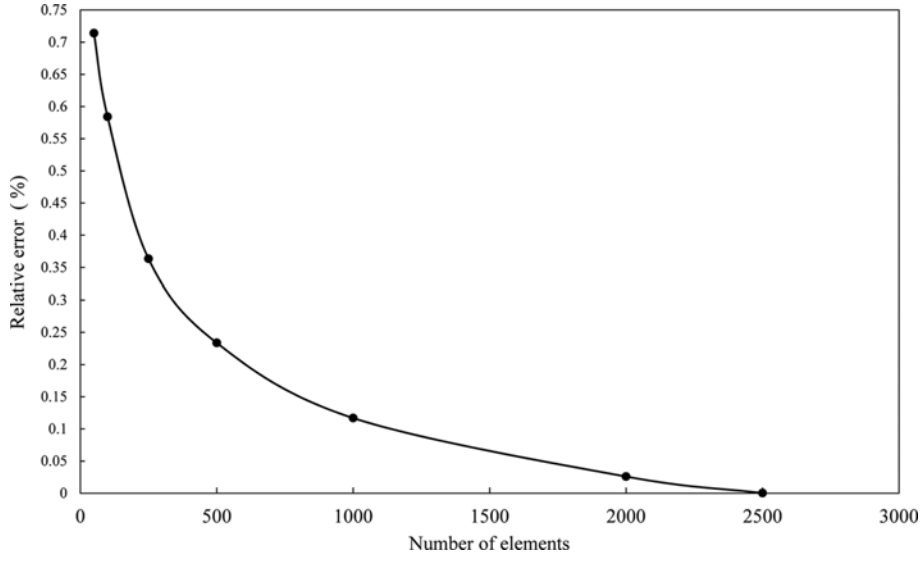

Fig. 3. Grid independency check results.

Table 2. The specifications of the modules and set of experimental data used for model validations and analysis

Input parameter	Unit	O_2/N_2 separation		CO_2/CH_4 separation
Mole fraction in feed	-	0.205 O_2 0.795 N_2	0.2078 O_2 0.7922 N_2	0.6 CO_2 0.4 CH_4
Feed pressure	atm	7.8	6.82	2, 4, 7
Permeate outlet pressure	atm	1	1.01	1
Feed temperature	K	296.15	298.15	298.15 338.15
Activation energy	$kJ \cdot mol^{-1}$	19.3 O_2 27.6 N_2	19.3 O_2 27.6 N_2	17.765 CO_2 15.468 CH_4
Inner fiber diameter	μm	80	145	389
Outer fiber diameter	μm	160	373	735
Module diameter	mm	9.5	4.8	10
Number of fiber	-	368	80	100
Active fiber length	cm	25	75	15
Ref.	[50]	[17]	[49]	

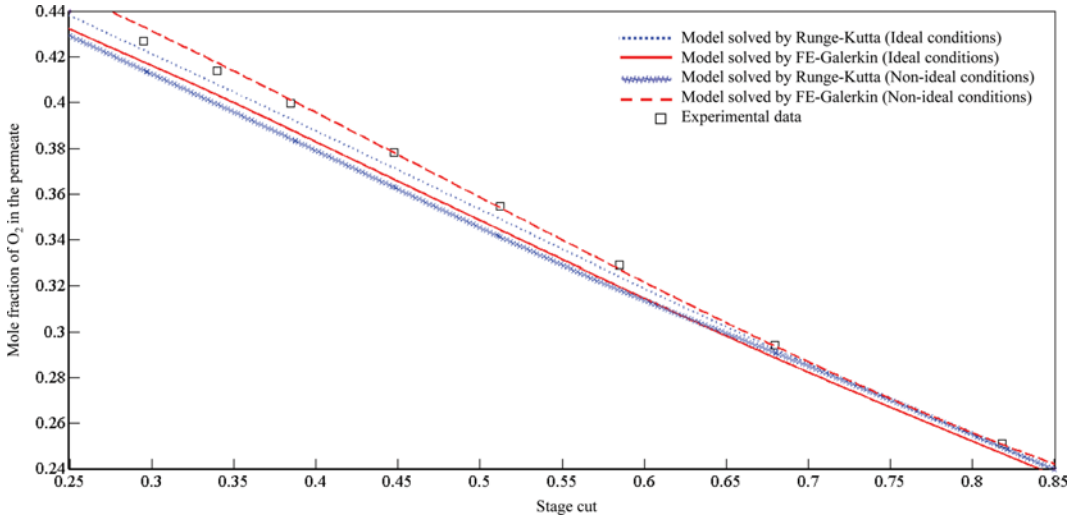

Fig. 4. The results of modeling transport based on ideal and non-ideal conditions and the effect of solution method in the case O_2/N_2 separation (P_F=7.8 atm; T_F=296.15 K; experimental data from Ref. [50]).

cal results were grid-independent. The results are shown in Fig. 3 in the case of a binary CO_2/CH_4 gas mixture having a composition of 60% CO_2 flowing in the shell-side of a stainless steel cylindrical module with 15 cm length and 1 cm internal diameter housing 100 hollow fibers with internal and external diameters of 389 μm and 735 μm, respectively. The pressure difference between the feed and permeate sides was 6 atm and the feed temperature was 298 K. The trend in Fig. 3 reveals that the relative error was reduced exponentially by increasing in the number of grid elements. It was noted that the relative error reduced to less than 0.02% for the number of elements exceeding 2000. Therefore, the number of grid elements was set to 2000 for all the computations in this study.

2. Model Validation

Three exemplary case studies on O_2/N_2 and CO_2/CH_4 separations were investigated to examine how the numerical results obtained by the developed mathematical models compared to the experimental data. Table 2 represents the set of experimental data related to the case studies that were employed for the model validation. In the case of O_2/N_2 separation, hollow fiber composite membranes were from Alberta Research Council (ARC) [50] and Innovative Membrane Systems of Norwood, MA [17]. Also, for CH_4/CO_2 separation, hollow fiber composite membranes consisting of coating (aliphatic copolymer) and support (polysulfone) layers from SNIA were examined [49].

Fig. 4 shows the results obtained from the models developed based on ideal and non-ideal conditions and solved using FE-Galerkin and Runge-Kutta methods in the case of O_2/N_2 separation. In this figure, the mole fraction of O_2 in the permeate is plotted versus stage cut and compared to the experimental data reported by Feng et al. [50]. Results show that the predictions made by both ideal and non-ideal models solved using either FE-Galerkin or Runge-Kutta methods are generally in a good agreement with the experimental data. Focusing on the use of the Runge-Kutta method, the model developed based on ideal conditions provides a better match

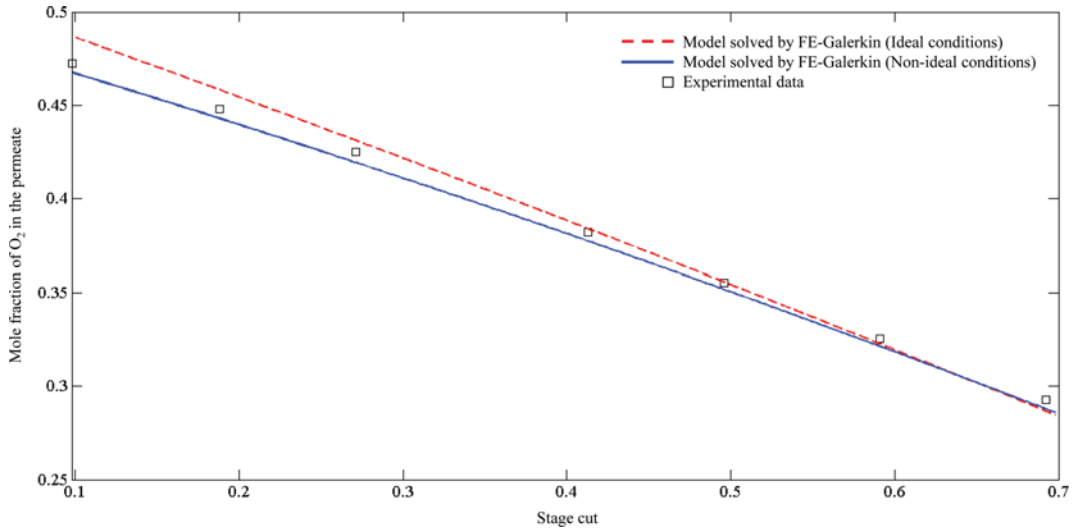

Fig. 5. The results of modeling transport based on ideal and non-ideal conditions solved using FE-Galerkin method in the case O_2/N_2 separation (P_F=6.82 atm; T_F=298.15 K; experimental data from Ref. [17]).

with the experimental data than the model incorporating non-ideal conditions. At the first glance, this may potentially be attributed to the intrinsically close-to-ideal properties of O_2 and N_2 molecules as well as the relatively low operational pressure, both promoting the system to behave with negligible deviations from ideal conditions. However, further insights considering solution using FE-Galerkin method reveal that the model incorporating non-ideal conditions provides better predictions than the model developed based on ideal conditions. Thus, the predictions by the non-ideal model solved using the FE-Galerkin method are in the best match with the experimental data. These findings suggest the lower accuracy of 4^{th} order Runge-Kutta compared to the FE-Galerkin method, highlighting the prominent role of adoption of an appropriate solution method. Interestingly, the predictions by both models become similar and regardless of the solution method at stage cuts beyond 0.7. This may be attributed to the lesser deviations of the O_2/N_2 gas mixture from ideal conditions at higher stage cuts.

Investigations were further extended by applying the approach in the case of another set of data reported by Giglia et al. for O_2/N_2 separation [17]. Fig. 5 presents the mole fraction of O_2 in the feed at different stage cuts for the models developed based on ideal and non-ideal conditions solved using the FE-Galerkin method. The results reveal that the predictions made by both models are in an admissible agreement with the experimental data. However, predictions by non-ideal model are in higher accuracy over the full range of stage cuts. Similar to the previous case, the accuracy of the predictions obtained by both ideal and non-ideal models approaches each other at higher stage cuts.

The validity of the models was also examined in case of CO_2/CH_4 separation by comparing to the experimental data reported

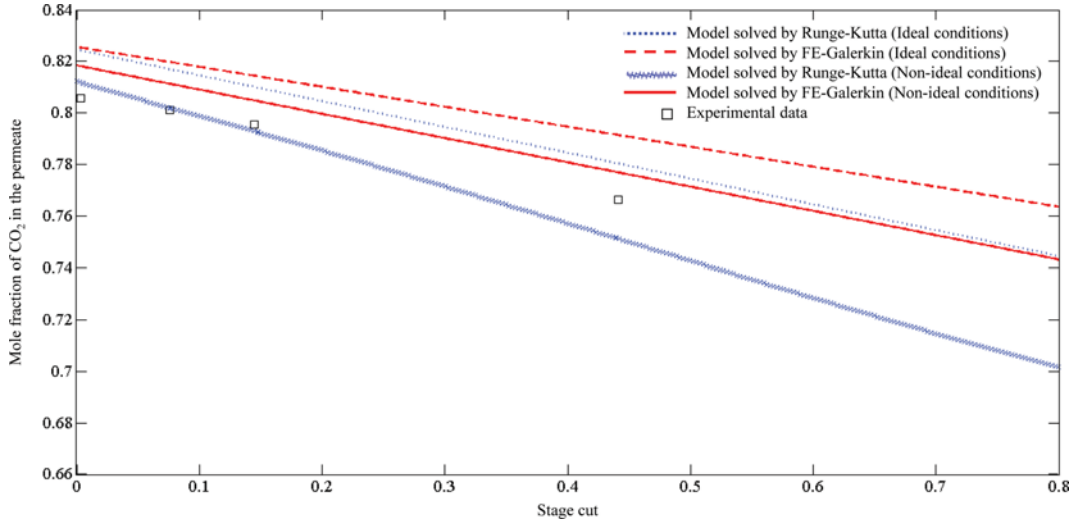

Fig. 6. The results of modeling transport based on ideal and non-ideal conditions and the effect of solution method in the case CO_2/CH_4 separation (P_F=7 atm; T_F=298.15 K; experimental data from Ref. [49]).

in literature [49]. Fig. 6 demonstrates the experimental as well as predicted values obtained by both models based on the mole fraction of CO_2 in the permeate stream at various stage cuts. Regardless of the solution method, essentially non-ideal model provides better predictions about the trend of changes in the mole fraction of CO_2 than the ideal model. Note that in contrast to the case of O_2/N_2 separation, the deviation between the predictions and experimental data increased upon increase in the stage cut in the case of CO_2/CH_4. In addition, the non-ideal model solved using FE-Galerkin method provided more accurate prediction than being solved using Runge-Kutta method. Especially, the predicted values by the non-ideal model solved using Runge-Kutta method deviated more as stage cut increased, whereas the non-ideal model solved by FE-Galerkin method followed the trend of experimental data to an acceptable level. In overall, the results suggest the higher accuracy of the FE-Galerkin compared to the Runge-Kutta method.

According to Figs. 4-6, it is clear that for the case of O_2/N_2, predictions by both ideal and non-ideal models are very similar and approach each other, especially at higher stage cuts. This may be attributed to the intrinsic properties of nonpolar gases like O_2 and N_2 which display nearly ideal behavior at ordinary pressures and temperatures. For natural gas separation, however, this trend is different. The model incorporating the non-ideal conditions provides more accurate predictions than the model developed based on ideal conditions due to the role of important non-idealities like concentration polarization. It is demonstrated that for a mixture containing a condensable gas like CO_2 and considering the distinct size difference between the CO_2 and CH_4 molecules, the effect of plasticization accelerates the diffusivity of the penetrants due to swelling of the polymer matrix [16,51]. In addition, the thin selec-

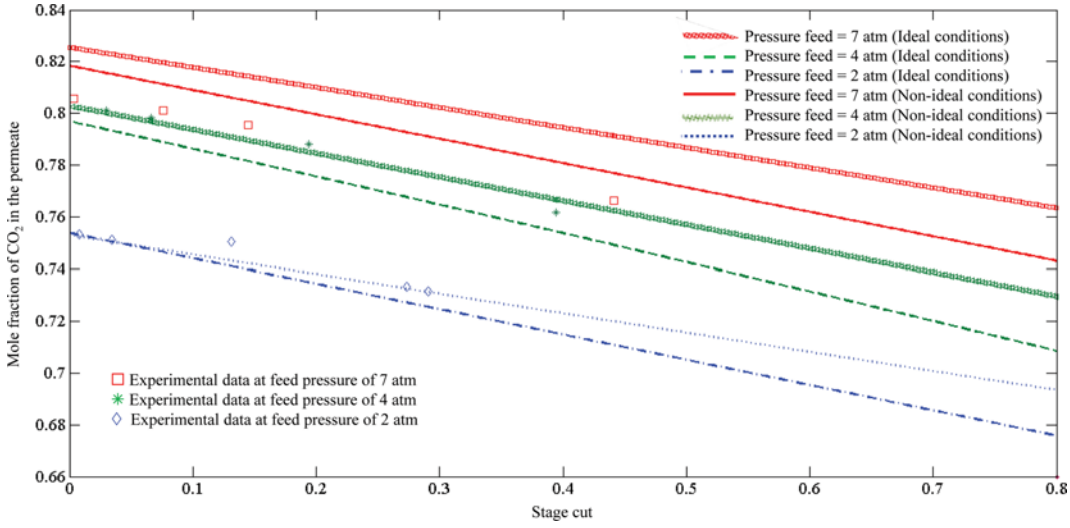

Fig. 7. The results of modeling transport based on ideal and non-ideal conditions and the effect of solution method in the case CO_2/CH_4 separation (T_F=298.15 K; experimental data from Ref. [49]).

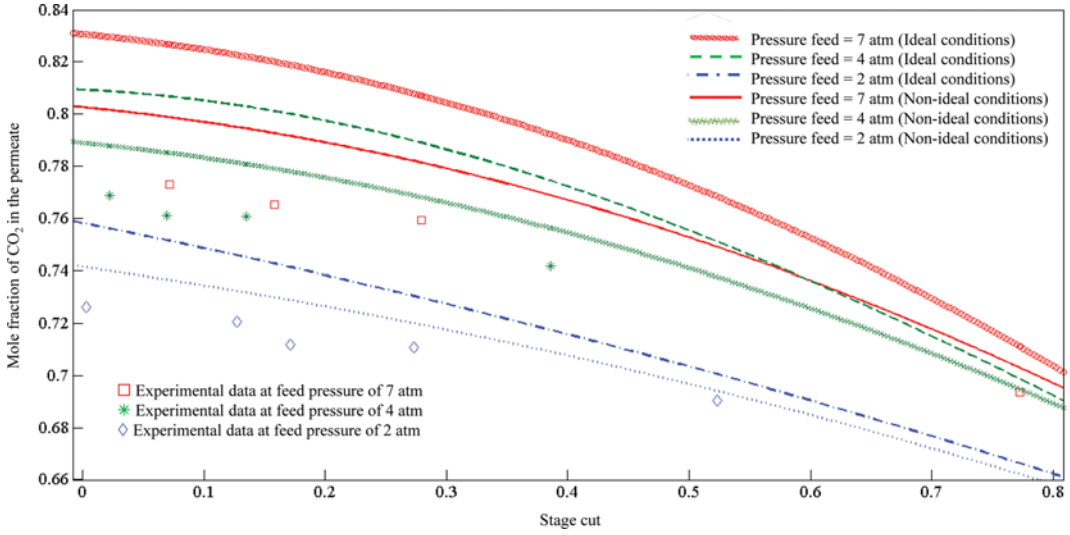

Fig. 8. The results of modeling transport based on ideal and non-ideal conditions and the effect of solution method in the case CO_2/CH_4 separation (T_F=338.15 K; experimental data from Ref. [49]).

Table 3. The parameters and levels used for sensitivity analysis based on operating conditions

Parameter	Unit	−1 Level	+1 Level	−alpha	+alpha
Feed pressure	atm	5.64	16.35	2	20
Feed temperature	K	303.28	333.01	293	343
Mole fraction of CO_2 in feed	-	0.3216	0.6783	0.2	0.8

Table 4. The parameters and levels used for sensitivity analysis based on physical geometries

Parameter	Unit	−1 Level	+1 Level	−alpha	+alpha
Fiber inner diameter	μm	275	425	200	500
Module diameter	cm	20	40	10	50
Number of fibers	-	1288	3673	50	5000
Active fiber length	cm	32.5	77.5	10	100

tive layer of the asymmetric hollow fiber promotes the plasticization to occur at low pressures [52]. Also, according to the solution-diffusion mechanism, the competition of CO_2 and CH_4 in the mixture for the limited sites within the membrane (known as competitive sorption) results in decreased CH_4 solubility. However, the increase in CH_4 diffusivity is much greater than the decrease in solubility, so that in overall, the permeability of CH_4 increases [53]. Consequently, it is expected that the deviation of model predictions from the experimental data in the case of CO_2/CH_4 mixture will be more than that of O_2/N_2 mixture.

Further investigations were carried out to examine the effect of pressure and temperature on the predictions by the developed models. Based on the findings, FE-Galerkin method was selected as the solution method. Figs. 7 and 8 show the effect of variation in the feed pressure on the mole fraction of CO_2 in the permeate stream at different stage cuts for two temperatures. Data in Fig. 7 and 8 are for the pressures of 2, 4 and 7 atm at 298.15 K and 338.15 K, respectively. According to Fig. 7, the model developed based on non-ideal conditions provides predictions with higher accuracy compared to the ideal model. This can be because the effect of non-idealities is more in the case of CO_2/CH_4 separation. Almost similar results can be observed in Fig. 8, which is related to the 338.15 K, corroborating the higher accuracy of the non-ideal model than the ideal one in predicting the performance. However, the accuracy of the predictions by the non-ideal model declined in the case of 338.15 K. On the other hand, essentially, the models are expected to offer more accurate results at lower pressures, since deviation between the experimental data and model predictions increases at higher pressures.

Generally, the above findings confirm the complexity of non-idealities involved in modeling the performance of permeators and the prominent role of inclusion of appropriate parameters to account for the elevated pressure and temperatures. Also, the concentration of the more permeable components at the permeate outlet reduced upon increase in stage cuts, illustrating the trade-off between the selectivity and stage cut. The effect was more pronounced as deviations from ideality increased.

3. Sensitivity Analysis

Sensitivity analysis was performed using the model comprising non-idealities aimed at investigating the main parameters and interactions affecting the results in the case of CO_2/CH_4 separation. Table 3 shows the parameters in terms of alpha and the levels of feed pressure, feed temperature and mole fraction of CO_2 in feed comprising operating conditions. Also, Table 4 shows the parameters in terms of alpha and the levels of fiber inner diameter, module diameter, number of fibers and active fiber length as physical geometries. The corresponding responses are presented in Tables 5 and 6.

Table 5. CCD parameters and mole fraction of CO_2 in permeate based on operating conditions

Run	Feed pressure (atm)	Feed temperature (K)	Mole fraction of CO_2 in feed	Mole fraction of CO_2 in permeate
1	11	343.15	0.5	0.7385
2	16.35	303.28	0.6783	0.8562
3	11	318.15	0.5	0.7304
4	11	318.15	0.8	0.9213
5	16.35	303.28	0.3216	0.5494
6	11	318.15	0.5	0.7304
7	11	318.15	0.5	0.7304
8	5.64	333.01	0.6783	0.8501
9	11	293.15	0.5	0.7207
10	5.64	333.01	0.3216	0.5279
11	11	318.15	0.5	0.7304
12	11	318.15	0.2	0.3791
13	11	318.15	0.5	0.7304
14	11	318.15	0.5	0.7304
15	20	318.15	0.5	0.7372
16	2	318.15	0.5	0.6313
17	5.64	303.28	0.3216	0.5178
18	5.64	303.28	0.6783	0.8432
19	16.35	333.01	0.3216	0.5618
20	16.35	333.01	0.6783	0.8632

Among the possible regression models, the quadratic type model was employed for the analysis of the results. Eqs. (23) and (24) represent the dependency of the mole fraction of CO_2 on the parameters involved in operating conditions and physical geometries, respectively:

Table 6. CCD parameters and mole fraction of CO_2 in permeate based on physical geometries

Run	Fiber inner diameter (μm)	Module diameter (cm)	Number of fibers	Active fiber length (cm)	Mole fraction of CO_2 in permeate
1	350	30	2525	10	0.8052
2	350	30	2525	100	0.7846
3	425	40	3763	77.5	0.7804
4	500	30	2525	55	0.7956
5	275	40	1288	32.5	0.8038
6	350	30	2525	55	0.7956
7	200	30	2525	55	0.7956
8	350	30	2525	55	0.7956
9	425	40	1288	32.5	0.8039
10	425	20	1288	32.5	0.8039
11	275	20	3763	32.5	0.7971
12	350	30	2525	55	0.7956
13	275	20	1288	77.5	0.7990
14	425	20	1288	77.5	0.7991
15	350	30	2525	55	0.7956
16	350	30	2525	55	0.7956
17	350	30	5000	55	0.7822
18	425	20	3763	32.5	0.7971
19	350	30	2525	55	0.7956
20	275	40	3763	32.5	0.7971
21	275	40	3763	77.5	0.7804
22	275	20	3763	77.5	0.7804
23	425	40	3763	32.5	0.7971
24	275	40	1288	77.5	0.7990
25	425	40	1288	77.5	0.7990
26	350	10	2525	55	0.7956
27	350	30	2525	55	0.7956
28	350	50	2525	55	0.7956
29	275	20	1288	32.5	0.8038
30	425	20	3763	77.5	0.7804

$$y=-2.54827-0.12763P_F+0.015643T_F+5.668797x_F+0.000428P_FT_F+0.0302P_Fx_F-0.01313T_Fx_F-0.00074P_F^2-2.3e-5T_F^2-1.0436x_F^2 \quad (23)$$

$$y=0.80434+1.67e-6N+7.34e-5L-1.07e-7NL-1.77e-10N^2-3.62e-7L^2 \quad (24)$$

These quadratic models have the least P-values. P-value is a significance check parameter that its smaller value means it is more significant [54]. Essentially, values of Prob>F less than 0.0500 indicate that model terms are significant. Based on the above results, the analysis of variance for the responses of quadratic model is presented in Tables 7 and 8 for operating conditions and physical geometries, respectively. In these tables, the sum of squares was taken based on the deviations from the mean value. Also, the number of terms added to the statistical quadratic model was defined by degree of freedom and F was defined by dividing sum of squares divided by the degree of freedom. Cor Total is the corrected total sum of squares representing the total amount of variations to the mean value. According to Table 7, the P-value probes corresponding to the input parameters were in the acceptable range, indicating the validity of the statistical model. According to Table 8, F, G, FG, F^2 and G^2 were significant model terms in the case of physical geometries and were considered in the model. However, values greater than 0.1000 indicate insignificant model terms, thus corresponding variables were excluded from the model to avoid unnecessary complexity.

According to Eq. (23), the mole fraction of the more permeable component in feed had the most effect on the mole fraction of CO_2 in the permeate stream. Also, the statistical model showed that the interaction between feed pressure and mole fraction of CO_2 was considerable. On the other hand, the negative quadratic effect of mole fraction of CO_2 in feed may have had a significant effect.

Considering physical geometries and with the aid of Eq. (24), the number of fibers and active fiber length had the most important effect on the results. The number of fibers has a direct influence on packing density and worth optimization. In fact, a large number of fibers can result in excessive pressure drop, whereas the

Table 7. Analysis of variance for mole fraction of CO_2 in permeate based on operating conditions

Source	Sum of squares	Degree of freedom	Mean square	F-value	P-value Prob>F	Status
Model	0.3342	9	0.0371	18.5704	<0.0001	Significant
Feed pressure (A)	0.0213	1	0.0213	10.6657	0.0085	
Feed temperature (B)	0.0030	1	0.0030	1.51883	0.2460	
Feed mole fraction of CO_2 (C)	0.2636	1	0.2636	131.8630	<0.0001	
AB	0.0092	1	0.0092	4.6382	0.0567	
AC	0.0066	1	0.0066	3.3240	0.0983	
BC	0.0097	1	0.0097	4.8518	0.0522	
A^2	0.0064	1	0.0064	3.2295	0.1025	
B^2	0.0004	1	0.0003	0.1901	0.6721	
C^2	0.0159	1	0.0158	7.9471	0.0182	
Residual	0.0199	10	0.0020			
Lack of fit	0.0199	5	0.0039			
Pure error	0	5	0			
Cor total	0.3542	19				

Table 8. Analysis of variance for mole fraction of CO_2 in permeate based on physical geometries

Source	Sum of squares	Degree of freedom	Mean square	F value	P-value Prob>F	Status
Model	0.0018	14	0.0001	4051.506	<0.0001	Significant
Fiber inner diameter (D)	3.75E-09	1	3.75E-09	0.1203	0.7335	
Module diameter (E)	4.17E-10	1	4.17E-10	0.0133	0.9095	
Number of fibers (F)	0.0009	1	0.0009	30442.26	<0.0001	
Active fiber length (G)	0.0007	1	0.0007	21664.83	<0.0001	
DE	6.25E-10	1	6.25E-10	0.020053	0.8893	
DF	5.62E-09	1	5.62E-09	0.1804	0.6770	
DG	6.25E-10	1	6.25E-10	0.0200	0.8893	
EF	6.25E-10	1	6.25E-10	0.0200	0.8893	
EG	6.25E-10	1	6.25E-10	0.0200	0.8893	
CD	0.0001	1	0.0001	4524.5666	<0.0001	
D^2	3.6E-09	1	3.6E-09	0.1155	0.7386	
E^2	3.6E-09	1	3.6E-09	0.1155	0.7386	
F^2	2.06E-06	1	2.06E-06	66.0513	<0.0001	
G^2	9.54E-07	1	9.54E-07	30.5968	<0.0001	
Residual	0.0199	10	0.0020			
Cor total	0.3542	19				

surface area required for permeation is decreased by decreasing the number of fibers.

The accuracy of any model could be checked by various measures. In the case of physical geometries and operating conditions, the obtained R-Squared factors were 0.9997 and 0.8132 and the Adj R-Squared factors were 0.9995 and 0.7782, respectively. Both R-Squares and Adj R-Squares were in reasonable agreement. Further investigations were carried out and the predicted results obtained through application of statistical models were plotted versus actual data obtained from the numerical model comprising non-ideal conditions. According to Fig. 9, the aggregation of points along the straight line corroborated the validity of the statistical models. On the other hand, Fig. 10 represents the plot of statistical model residuals versus predicted results, revealing randomly scattered residuals fit the variance satisfactorily.

As presented earlier, at constant operating conditions, the number of fibers and active fiber length had the most influence on the predicted mole fraction of CO_2 in the permeate stream. Fig. 11 represents the three-dimensional response surfaces of mole fraction of CO_2 in the permeate stream as a function of both active fiber length and the number of fibers in the module. According to Fig. 11(a), the maximum mole fraction of CO_2 in the permeate stream was observed when the active fiber length and number of fibers were small and mole fraction of CO_2 in the permeate stream increased from 0.7971 to 0.8038 (~1%) by decreasing the number of hollow fibers having length of 32.5 cm. A greater increase (~2.3%) was achieved in the case of fibers having length of 77.5 cm. Fig. 11(b) provides more insights by showing that at any constant fiber length, increasing the number of fibers decreased the mole fraction of CO_2 in the permeate stream. Although this effect is advantageous

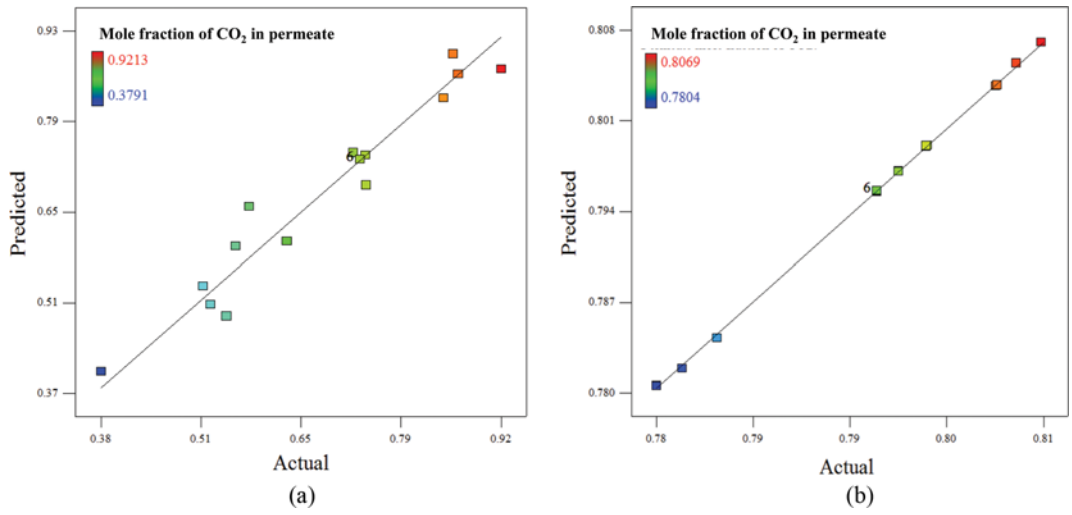

Fig. 9. Predicted (statistical model) mole fraction of CO_2 in permeate versus Actual (numerical model) for (a) operating conditions (b) physical geometries.

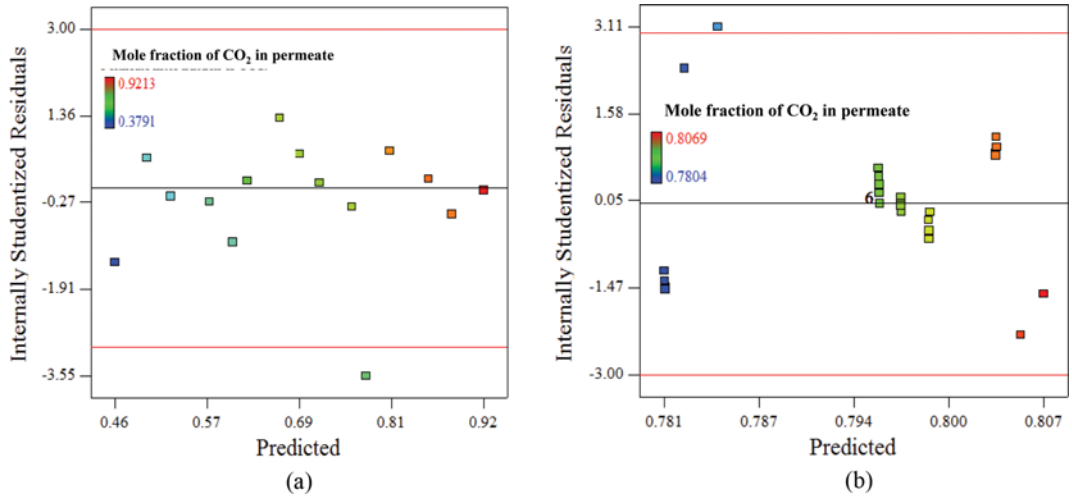

Fig. 10. Internal residuals versus predicted (statistical model) for mole fraction of CO_2 in the permeate for (a) operating conditions (b) physical geometries.

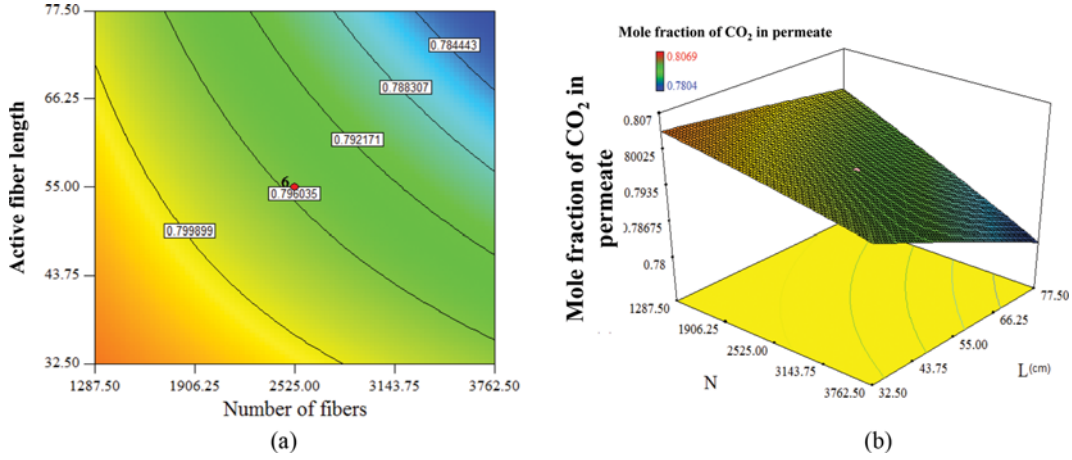

Fig. 11. (a) Contour plot and (b) 3D response surface of the interactive effect for the mole fraction of CO_2 in permeate: Effects of active fiber length (L) and number of fibers (N).

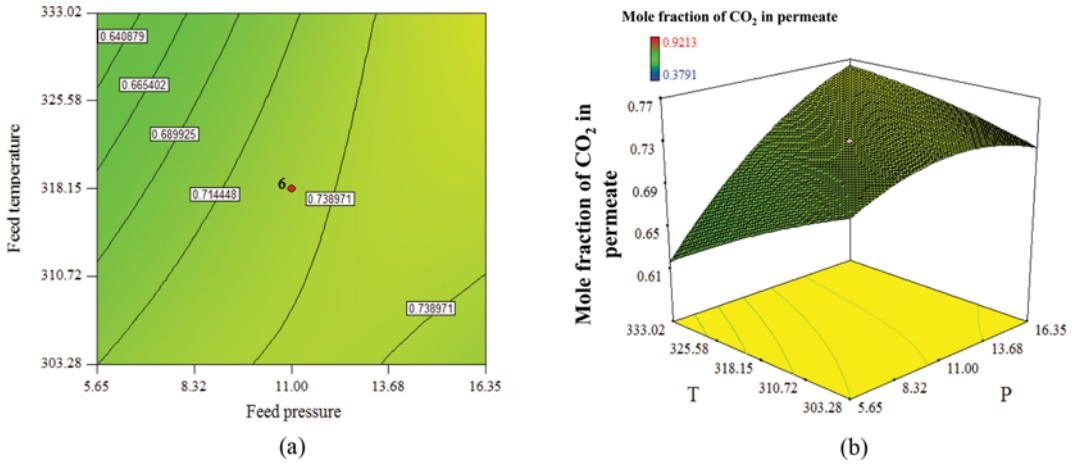

Fig. 12. (a) Contour plot and (b) 3D response surface of the interactive effect for the mole fraction of CO_2 in permeate: Effects of feed temperature (T) and feed pressure (P) at constant feed composition.

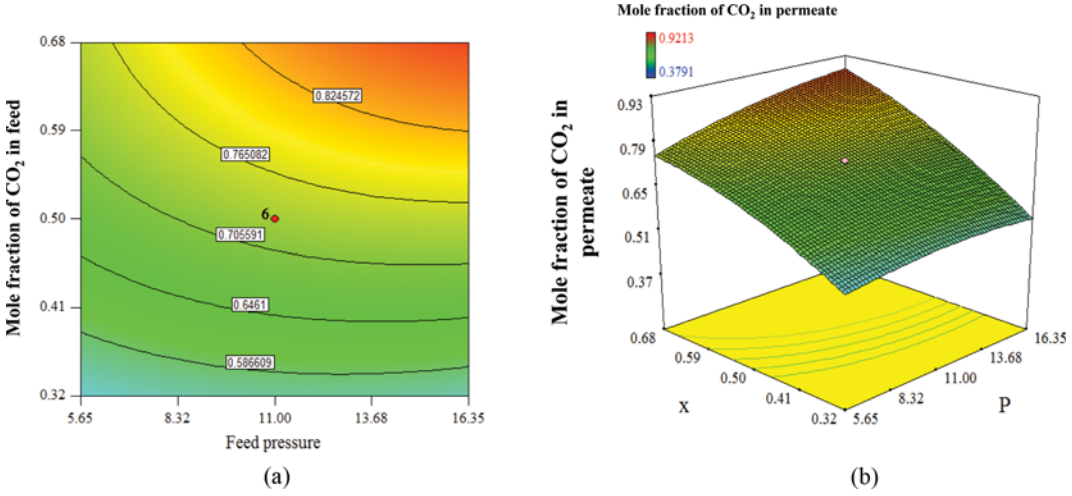

Fig. 13. (a) Contour plot and (b) 3D response surface of the interactive effect for the mole fraction of CO_2 in permeate: Effects of feed composition (x) and feed pressure (P) at constant feed temperature.

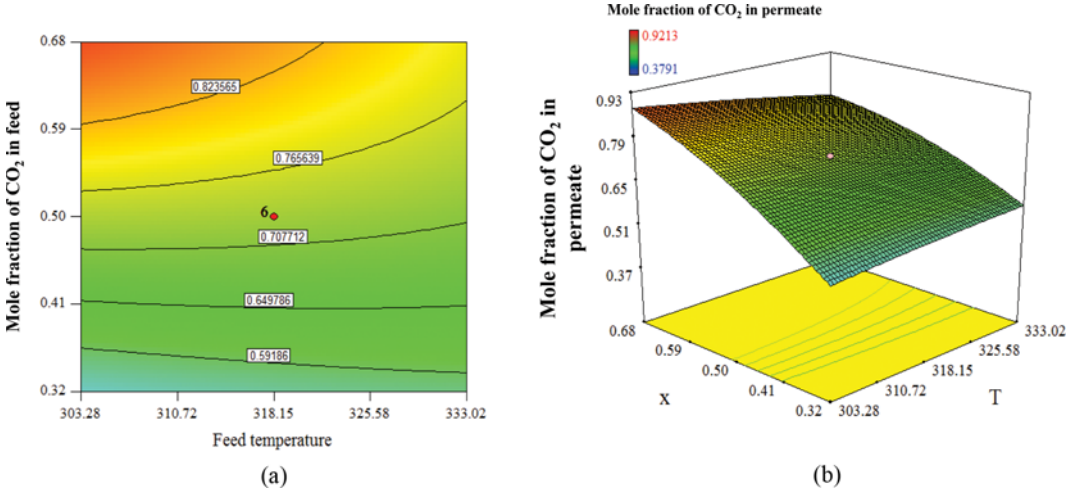

Fig. 14. (a) Contour plot and (b) 3D response surface of the interactive effect for the mole fraction of CO_2 in permeate: Effects of feed composition (x) and feed temperature (T) at constant feed pressure.

in terms of permeation surface area, the increased pressure drop along the fibers results in decreased driving force between lumen- and shell-sides and subsequently, reduces the mole fraction of CO_2 in the permeate stream. Results also show that considering a constant number of fibers, increasing the length of fiber is not always favorable, since by increasing the length of fibers the initial desired driving force for overcoming the resistances of the membrane layers may not be sufficient. For instance, the mole fraction of more permeable component in the permeate stream decreased from 2% to 0.6% by increasing the length of fibers from 32.5 to 77.5 cm. This decrease may be explained by the fact that in the absence of desired driving force, which mostly is related to the feed pressure, increasing the length of fibers provides a good chance for the less permeable component to pass through the membrane surface more favorably and diminish selectivity.

Figs. 12, 13 and 14 depict variations in mole fraction of CO_2 in the permeate stream by considering operating conditions as input variables in the statistical model. According to Fig. 12, it could be realized that at lower temperatures, increasing feed pressure initially increased the mole fraction of CO_2 in the permeate stream. However, the mole fraction of CO_2 declined upon further increase in feed pressure to ~12 atm. It is known that at low pressures the permeance is reduced due to dominance of competitive sorption of the components. Increasing feed pressure improves the available driving force across the membrane so that transport of CO_2 is decreased after a given pressure due to accretion of CH_4 through the membrane. In addition, at 333.02 K, 19.6% increase in mole fraction of CO_2 in the permeate stream was observed by increasing pressure. In upper ranges of feed temperature, always increasing the feed pressure increases desired driving force so that the mole fraction of CO_2 in the permeate stream increases. Therefore, the results reveal that interactions of feed pressure and temperature play important roles in the trends. By considering feed at pressure of 5.65 atm, a decrease of 9.55% in mole fraction of CO_2 in the permeate stream occurred by increasing feed temperature, while using feed at pressure of 16.35 atm resulted in 6.2% increase in mole fraction of CO_2 in the permeate stream. Considering low feed pressures, the increase in permeance of CH_4 upon increase in feed temperature could hamper the available driving force for CO_2 permeability, and accordingly CH_4 molecules permeate more. Another important point is that according to Fig. 12, feed pressure compared to temperature has more influence on the trends.

Fig. 13 demonstrates that both feed composition and pressure have direct influences on the mole fraction of CO_2 in the permeate stream. For a given hollow fiber module, increasing the mole fraction of CO_2 in the feed increased the driving force of CO_2 permeation, whereas the driving force for CH_4 permation declined. It is also evident from the same figure that at a constant pressure, by increasing the mole fraction of CO_2 in the feed, its mole fraction in permeate stream increased by 42.62% and 62.19% at feed pressure of 5.65 atm and 16.35 atm, respectively. Also at a given feed compostion, by increasing the feed pressure the available driving force across the membrane surface as well as the selectivity increased. The mole fraction of CO_2 in the permeate stream increased about 5.9% and 18.9% for CO_2 mole fraction of 0.32 and 0.68 in the feed, respectively.

Fig. 14 explains the effects of feed composition and temperature on the mole fraction of CO_2 in the permeate stream. At all ranges of temperature, increasing the mole fraction of CO_2 in the feed increased its mole fraction in the permeate. This increase was more at lower feed temperatures. According to Fig. 14, the mole fraction of CO_2 in the permeate stream increased about 6.21% and 4.3% at feed temperatures of 303.28 and 333.02 K, respectively. For a given feed temperature, increasing the mole fraction of CO_2 in the feed increased the permeation driving force for CO_2, whereas the permeation driving force for CH_4 reduced. In addition, at lower ranges of the mole fraction of CO_2 in the feed, increasing feed temperature increased the mole fraction of CO_2 in the permeate stream steadily (about 3.4%). At higher ranges of mole fraction of CO_2 in the feed, increasing feed temperature was more effective on permeance of CH_4 and subsequently the purity of CO_2 decreased at the higher temperatures. Accordingly, the mole fraction of CO_2 in the permeate stream decreased about 7.9%.

4. Optimization

Generally, optimization involves finding the best solution or method from a set of applicable solutions [55]. For this purpose,

Table 9. Predicted mole fraction of CO_2 in permeate and verification of responses at optimum values for operating conditions

Feed pressure (atm)	Feed temperature (K)	Mole fraction of CO_2 in feed	Mole fraction of CO_2 in permeate (statistical model)	Desirability	Mole fraction of CO_2 in permeate (numerical model)	Error (%)
16.35	333.02	0.39	0.6659	0.7070	0.6800	2.07
16.35	333.02	0.42	0.6972	0.7659	0.7071	1.43
16.35	333.01	0.47	0.7402	0.8160	0.7481	1.06
16.35	333.01	0.52	0.7779	0.8577	0.7848	0.87
16.35	320.61	0.59	0.8258	0.9076	0.8265	0.08
14.77	303.29	0.65	0.8739	0.9553	0.8558	2.07

Table 10. Predicted mole fraction of CO_2 in permeate and verification of responses at optimum values for physical geometries

Fiber inner diameter (μm)	Module diameter (cm)	Number of fibers	Active fiber length (cm)	Permeate mole fraction of CO_2 (statistical model)	Desirability	Permeate mole fraction of CO_2 (numerical model)	Error (%)
424.95	22.34	1288	32.5	0.8038	0.8826	0.8134	1.19

the optimal values of input variables were obtained using statistical models. Note that for optimization of operating conditions, a set of feed composition variables was selected as the target. Tables 9 and 10 demonstrate the optimum conditions.

From Tables 9 and 10, it is clear that the values are in a correspondent agreement with the 3D surface plots. To verify the validity of statistical optimum conditions, values were employed to obtain the mole fraction of CO_2 using the model comprising non-idealities. The last two columns of Tables 9 and 10 represent the mole fraction of CO_2 in the permeate stream obtained by the numerical methods and the respective relative errors, respectively. The goal was to achieve the maximum difference between the mole fraction of CO_2 in feed and permeate. Results indicated a maximum error of 2.07% for the mole fraction of CO_2 in permeate stream. Table 9 shows optimum values for operating conditions set at feed pressure of 16.35 atm, feed temperature of 333.02 K and feed composition in the range of 39 to 52%. Also, Table 10 provides the optimum values for physical geometries yielded permeate mole fraction of 0.8134 for CO_2.

CONCLUSIONS

Mathematical models describing the performance of hollow fiber membrane modules were developed for separation of binary gas mixtures. The effects of major non-ideal and ideal conditions were taken into account in mathematical modeling and the influences on the final results were investigated in detail. The validity and accuracy of the models solved using Runge-Kutta and finite element methods were examined and compared to the experimental data. Results highlight the important role of employing an appropriate numerical method. Also, findings reveal that the model incorporated non-ideal conditions, solved using the FE-Galerkin method, could offer the closest predictions to the experimental data. The model incorporating non-ideal effects and the model developed based on ideal conditions both offered reliable predictions at higher stage cuts in the case of O_2/N_2. However, the model incorporating non-ideal effects fitted experimental data well at lower pressures in the case of CO_2/CH_4. However, the gas mixture deviated more from ideal conditions upon increasing the feed pressure, leading to slight overestimations compared to the experimental data. In addition, the effects of operating conditions and physical geometries on the performance of hollow fiber membrane permeators were investigated through sensitivity analysis, and optimum conditions were obtained through statistical analysis. Findings revealed that feed composition and pressure as well as active fiber length and number of fibers were the most important input parameters that influence the separation performance. The presented models and results gained through sensitivity analysis provide useful information for design and development of high performance hollow fiber membrane permeators for gas separation applications.

ACKNOWLEDGEMENTS

Authors would like to thank Ms. Sara Najari (Tarbiat Modares University) and Dr. Nicolas R. Tan (HOSSTECH Group, Singapore) for their valuable contributions to this project.

NOMENCLATURE

Symbols

C_{pi} : molar heat capacity at constant pressure for component i [J/mol·K]
d_i : fiber inner diameter [m]
d_o : fiber outer diameter [m]
d_{s0} : module shell diameter [m]
E : activation energy for permeation through the membrane [J/mol]
f : friction factor
G : mass flux of feed-side stream [kg/s·m^2]
g_c : Newton's law conversion factor [kg·m/N·s^2]
k : mass transfer coefficient in the feed-side [m/s]
K_1, K_2 : dimensionless factors
L : active fiber length [m]
Mw_m : molecular weight of the gas mixture [kg/mole]
N : total number of hollow fibers in the hollow fiber module
P : pressure [Pa]
Q : permeability [mole/m^2·s·Pa]
R : ideal gas constant [J/mole·K]
R_h : hydraulic radius [m]
T : temperature [K]
U : retentate gas flow rate in the hollow fiber module [mole/s]
U^* : normalized retentate gas flow rate in the hollow fiber module
U_i : feed gas flow rate in the hollow fiber module [mole/s]
V : permeate gas flow rate in the hollow fiber module [mole/s]
V^* : normalized permeate gas flow rate in the hollow fiber module
x_F : feed mole fraction of the more permeable component
x_s : surface mole fraction of the more permeable component in the feed-side stream
y : permeate mole fraction of the more permeable component in the bulk permeate stream
y′ : local permeate-side mole fraction of the more permeable component in the membrane porous layer
z : hollow fiber length variable measured from the open end [m]
z^* : normalized hollow fiber length
Z : compressibility factor

Greek Letters

α : membrane selectivity
Γ : ratio of permeate side pressure to feed side pressure
δ : effective skin thickness of asymmetric membrane [m]
μ : viscosity of the gas mixture [Pa·s]
$\mu_{JT,i}$: Joule-Thomson coefficient of component i [K/Pa]
$\mu_{JT,m}$: Joule-Thomson coefficient of the gas mixture [K/Pa]
π : 3.1416
ϕ_{11} : fugacity coefficient of the more permeable component in the feed side
ϕ_{12} : fugacity coefficient of the more permeable component in the permeate side
ϕ_{21} : fugacity coefficient of the less permeable component in the feed side
ϕ_{22} : fugacity coefficient of the less permeable component in the

permeate side

Subscripts

0 : standard condition
a : more permeable component
b : less permeable component
F : feed side
i : open end of the fiber (feed inlet) or component *i*
j : component j
m : gas mixture
o : closed end of the fiber (retentate outlet)
P : permeate side
ref : reference

REFERENCES

1. S. S. Hosseini and T. S. Chung, *J. Membr. Sci.*, **328**, 174 (2009).
2. M. A. Alaei Shahmirzadi, S. S. Hosseini, G. Ruan and N. R. Tan, *RSC Adv.*, **5**, 49080 (2015).
3. S. S. Hosseini, Y. Li, T.-S. Chung and Y. Liu, *J. Membr. Sci.*, **302**, 207 (2007).
4. H. Kwon, M. Lu and J. Lee, *Korean J. Chem. Eng.*, **31**, 949 (2014).
5. S. S. Hosseini, M. R. Omidkhah, A. Zarringhalam Moghaddam, V. Pirouzfar, W. B. Krantz and N. R. Tan, *Sep. Purif. Technol.*, **122**, 278 (2014).
6. S. Najari, S. S. Hosseini, M. Omidkhah and N. R. Tan, *RSC Adv.*, **5**, 47199 (2015).
7. S. S. Hosseini and T. S. Chung, *Polymer blends and carbonized polymer blends*, in, Google Patents (2014).
8. J. K. Park and J. I. Seo, *Korean J. Chem. Eng.*, **19**, 940 (2002).
9. S. S. Hosseini, M. M. Teoh and T. S. Chung, *Polymer*, **49**, 1594 (2008).
10. T. Teerachaiyapat and P. Ramakul, *Korean J. Chem. Eng.*, **33**, 8 (2016).
11. S. Weller and W. A. Steiner, *J. Appl. Phys.*, **21**, 279 (1950).
12. S. S. Hosseini, N. Peng and T. S. Chung, *J. Membr. Sci.*, **349**, 156 (2010).
13. Q. T. Nguyen, R. Gref, R. Clément and H. Lenda, *Colloid Polym. Sci.*, **271**, 1134 (1993).
14. K. A. Fattah, S. M. Hamam, G. Al-Enezi, H. M. Ettoueny and R. Hughes, *J. Membr. Sci.*, **65**, 247 (1992).
15. P. K. Kundu, A. Chakma and X. Feng, *Can. J. Chem. Eng.*, **90**, 1253 (2012).
16. R. Wang, S. L. Liu, T. T. Lin and T. S. Chung, *Chem. Eng. Sci.*, **57**, 967 (2002).
17. S. Giglia, B. Bikson, J. E. Perrin and A. A. Donatelli, *Ind. Eng. Chem. Res.*, **30**, 1239 (1991).
18. B. J. Gornshteyn, *Can. J. Chem. Eng.*, **81**, 139 (2003).
19. A. F. Ismail and S. Haron, *Development of a simulation model for a hollow fiber membrane N2-H2 separation system*, Jurnal Teknologi, 45 (2000).
20. T. Katoh, M. Tokumura, H. Yoshikawa and Y. Kawase, *Sep. Purif. Technol.*, **76**, 362 (2011).
21. A. S. Kovvali, S. Vemury and W. Admassu, *Ind. Eng. Chem. Res.*, **33**, 896 (1994).
22. S. P. Lim, X. Tan and K. Li, *Chem. Eng. Sci.*, **55**, 2641 (2000).
23. J. Marriott and E. Sorensen, *Chem. Eng. Sci.*, **58**, 4975 (2003).
24. J. I. Marriott, E. Sorensen and I. D. L. Bogle, *Comput. Chem. Eng.*, **25**, 693 (2001).
25. S. Zhao, Z. Li, Y. Liu and L. e. Wang, *Desalination*, **233**, 310 (2008).
26. S. P. Kaldis, G. C. Kapantaidakis, T. I. Papadopoulos and G. P. Sakellaropoulos, *J. Membr. Sci.*, **142**, 43 (1998).
27. D. T. Coker, T. Allen, B. D. Freeman and G. K. Fleming, *AIChE J.*, **45**, 1451 (1999).
28. R. Khalilpour, A. Abbas, Z. Lai and I. Pinnau, *Chem. Eng. Res. Design*, **91**, 332 (2013).
29. P. K. Kundu, A. Chakma and X. Feng, *Can. J. Chem. Eng.*, **91**, 1092 (2012).
30. A. Makaruk and M. Harasek, *J. Membr. Sci.*, **344**, 258 (2009).
31. A. A. Shamsabadi, A. Kargari, F. Farshadpour and S. Laki, *J. Membr. Sep. Technol.*, **1**, 19 (2012).
32. C. Y. Pan, *AIChE J.*, **32**, 2020 (1986).
33. S. S. Hosseini, S. M. Roodashti, P. K. Kundu and N. R. Tan, *Can. J. Chem. Eng.*, **93**, 1275 (2015).
34. S.S. Hosseini, S. Najari, P. K. Kundu, N. R. Tan and S. M. Roodashti, *RSC Adv.*, **5**, 86359 (2015).
35. A. F. Ismail, H. Saidi and A. Abdul Rahman, Numerical solution of a mathematical model for hollow-fiber membrane gas separation system, in: Seminar Penyelidikan Fakulti Kej. Kimia & Kej. Sumber Asli, Jawatankuasa PenyelIdikan & Perundingan, Fakulti Kej. Kimia & Kej. Sumber Asli, UTM, 1 (1993).
36. C. Y. Pan, *AIChE J.*, **29**, 545 (1983).
37. V. Singh, R. R. Rhinehart, R. S. Narayan and R. W. Tock, *Ind. Eng. Chem. Res.*, **34**, 4472 (1995).
38. M. Scholz, T. Harlacher, T. Melin and M. Wessling, *Ind. Eng. Chem. Res.*, **52**, 1079 (2012).
39. J. A. Dehkordi, S. S. Hosseini, P. K. Kundu and N. R. Tan, *Chemical Product and Process Modeling*, **11**, 11 (2016).
40. S. S. Hosseini, J. A. Dehkordi and P. K. Kundu, *Chemical Product and Process Modeling*, **11**, 7 (2016).
41. J. M. Prausnitz, R. N. Lichtenthaler and E.G. de Azevedo, *Molecular thermodynamics of fluid-phase equilibria*, Pearson Education (1998).
42. H. Gorissen, *Chemical Engineering and Processing: Process Intensification*, **22**, 63 (1987).
43. B. E. Poling, J. M. Prausnitz and J. P. O'Connell, *The Properties of Gases and Liquids*, 5th Ed., McGraw-Hill Professional (2001).
44. B. Cockburn, G. E. Karniadakis and C.-W. Shu, *The development of discontinuous Galerkin methods*, Springer (2000).
45. A. Al-Omari, H.-B. Schuttler, J. Arnold and T. Taha, Solving Nonlinear Systems of First Order Ordinary Differential Equations Using a Galerkin Finite Element Method, Access, IEEE, **1**, 408 (2013).
46. S. Rastegar, S. Mousavi, M. Rezaei and S. Shojaosadati, *J. Ind. Eng. Chem.*, **20**, 3096 (2014).
47. A. Hassani, R. Darvishi Cheshmeh Soltani, M. Kıranşan, S. Karaca, C. Karaca and A. Khataee, *Korean J. Chem. Eng.*, **33**, 178 (2016).
48. R. H. Myers, D. C. Montgomery and C. M. Anderson-Cook, *Response surface methodology: process and product optimization using designed experiments*, John Wiley & Sons (2009).
49. L. Tranchino, R. Santarossa, F. Carta, C. Fabiani and L. Bimbi, *Sep. Sci. Technol.*, **24**, 1207 (1989).
50. X. Feng, J. Ivory and V. S. V. Rajan, *AIChE J.*, **45**, 2142 (1999).
51. E. Sanders, W. J. Koros, H. Hopfenberg and V. Stannett, *J. Membr.*

Sci., **18**, 53 (1984).
52. R. Chern, W. Koros, B. Yui, H. Hopfenberg and V. Stannett, *J. Polym. Sci.: Polym. Phys. Ed.*, **22**, 1061 (1984).
53. M. Donohue, B. Minhas and S. Lee, *J. Membr. Sci.*, **42**, 197 (1989).
54. V. Pirouzfar, S. S. Hosseini, M. R. Omidkhah and A. Z. Moghaddam, *Polym. Eng. Sci.*, **54**, 147 (2014).
55. G. Dantzig, *The nature of mathematical programming*, Mathematical Programming Glossary (2010).